JACS
JOURNAL OF THE AMERICAN CHEMICAL SOCIETY

ARTICLE

pubs.acs.org/JACS

Site, Rate, and Mechanism of Photoprotective Quenching in Cyanobacteria

Lijin Tian,[†] Ivo H. M. van Stokkum,[‡] Rob B. M. Koehorst,[†] Aniek Jongerius,[†] Diana Kirilovsky,[§] and Herbert van Amerongen[†,∥,*]

[†]Laboratory of Biophysics, Wageningen University, P.O. Box 8128, 6700 ET, Wageningen, The Netherlands

[‡]Biophysics Group, Department of Physics and Astronomy, Faculty of Sciences, VU University, DeBoelelaan1081, 1081 HV Amsterdam, The Netherlands

[§]Commissariat à l'Energie Atomique, Institut de Biologie et Technologies de Saclay and Centre National de la Recherche Scientifique, 91191 Gif sur Yvette, France

[∥]MicroSpectroscopy Centre, Wageningen University, P.O. Box 8128, 6700 ET, Wageningen, The Netherlands

Supporting Information

ABSTRACT: In cyanobacteria, activation of the Orange Carotenoid Protein (OCP) by intense blue-green light triggers photoprotective thermal dissipation of excess absorbed energy leading to a decrease (quenching) of fluorescence of the light harvesting phycobilisomes and, concomitantly, of the energy arriving to the reaction centers. Using spectrally resolved picosecond fluorescence, we have studied cells of wild-type *Synechocystis* sp. PCC *6803* and of mutants without and with extra OCP (ΔOCP and OverOCP) both in the unquenched and quenched state. With the use of target analysis, we managed to spectrally resolve seven different pigment pools in the phycobilisomes and photosystems I and II, and to determine the rates of excitation energy transfer between them. In addition, the fraction of quenched phycobilisomes and the rates of charge separation and quenching were resolved. Under our illumination conditions, ~72% of the phycobilisomes in OverOCP appeared to be substantially quenched. For wild-type cells, this number was only ~29%. It is revealed that upon OCP activation, a bilin chromophore in the core of the phycobilisome, here called APC^{Q}_{660}, with fluorescence maximum at 660 nm becomes an effective quencher that prevents more than 80% of the excitations in the phycobilisome to reach Photosystems I and II. The quenching rate of its excited state is extremely fast, that is, at least $(\sim 240 \pm 60 \text{ fs})^{-1}$. It is concluded that the quenching is most likely caused by charge transfer between APC^{Q}_{660} and the OCP carotenoid hECN in its activated form.

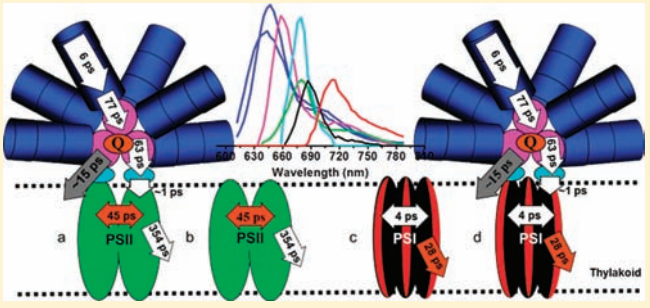

INTRODUCTION

Too much light can be lethal for photosynthetic organisms and it can for instance induce photo-oxidative damage of the reaction centers (RCs).[1−3] To protect themselves, plants, algae, and cyanobacteria have evolved protective mechanisms such as nonphotochemical quenching (qE in plants and qE_{cya} in cyanobacteria) to dissipate excess excited-state energy as heat.[4−6] The occurrence of qE_{cya} in the cyanobacterium *Synechocystis* sp. PCC *6803* (hereafter called *Synechocystis*) and the involvement of the large extra-membrane cyanobacterial antenna, the phycobilisome (PB), was first suggested by El Bissati et al. using strong blue-green light.[7] Later the action spectrum for qE_{cya} reported by Rakhimberdieva et al.[8] in a PSII-deficient mutant of *Synechocystis* suggested that blue-green light-activated carotenoids were involved in this mechanism. The involvement of the orange carotenoid protein (OCP) in qE_{cya} was next identified by Wilson et al.,[9] and it was found that a reversible conformational change of OCP from its inactive orange form (OCP^{o}) to its active red form (OCP^{r}), triggered by blue-green light, is responsible for qE_{cya}.[10] The conformational change is accompanied by a red shift of the absorption maximum of the OCP pigment, 3′hydroxyechinenone (hECN).[10] The activation of the OCP is a very low quantum yield reaction and it is light intensity dependent.[10] Only the OCP^{r} can bind to the PB and trigger the quenching of the PB.[11] Another protein called the Fluorescence Recovery Protein (FRP) is essential to recover the full antenna capacity under low-light conditions after exposure to high irradiance. This protein, by interacting with OCP^{r}, induces its conversion to OCP^{o} and helps the detachment of the OCP from the PB.[11,12] The process of qE_{cya} was investigated in numerous studies during the past few years.[8−20]

Genes encoding for homologues of the *Synechocystis* OCP are present in most PB-containing cyanobacteria and all these strains

Received: July 23, 2011
Published: October 05, 2011

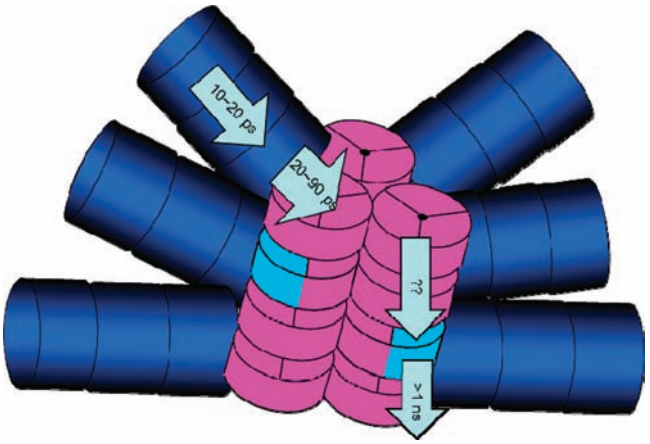

Figure 1. Schematic representation of a *Synechocystis* sp. PCC *6803* PB and previously determined excitation energy transfer times. Dark blue corresponds to C_PC (emitting at 640−650 nm), magenta to APC_{660} (emitting at 660 nma), and cyan to APC_{680} (emitting at ∼680 nm). The longest lifetime corresponds to decay to the ground state.

are able to perform qE_{cya}.[17] The quenching efficiency depends on the concentration of OCP. This was demonstrated by studying a mutant overexpressing OCP (OverOCP) that shows more quenching than the wild-type (WT) under the same high-light condition and a mutant not capable of synthesizing OCP (ΔOCP), which shows no quenching at all.[9,10] Note that in WT cells grown at low- or medium-light conditions the number of OCP's is lower than the number of PBs and presumably not all PBs can be quenched.[21] Nevertheless, even under these conditions, the qE_{cya} mechanism is photoprotective. The ΔOCP *Synechocystis* mutant is more sensitive to high-light conditions than the WT.[9] Moreover, cyanobacteria strains containing the OCP are more resistant to photoinhibition than strains lacking the OCP and the qE_{cya} mechanism.[17] Under stress conditions, like iron starvation, the ratio of OCP to phycobilisomes increases inducing a much larger energy and fluorescence quenching rendering the cells more resistant to environmental changes.[16]

The fluorescence recovery depends on the FRP to OCP ratio.[11] Thus, in WT cells, total fluorescence recovery is reached in only 10 min, while in the overOCP strain, more than 30 min are needed to recover the full antenna capacity at 32 °C. In addition, this reaction is largely temperature dependent: Below 10 °C, almost no recovery is observed.[10,14]

In *Synechocystis*, the light-harvesting PB contains six C-phycocyanin (C-PC) rods and three allophycocyanin (APC) core cylinders. Each C-PC rod is composed of three hexamer disks with a maximum absorbance at 620 nm and maximum fluorescence at 640−650 nm. Each APC cylinder contains four trimer discs with maximum absorbance at 650 nm. The two APC cylinders which are closest to the membrane contain two trimer discs formed by 3 $\alpha\beta$APC emitting at 660 nm (APC_{660}) and two trimers in which one of the α or the β APC subunits is replaced by a special subunit, ApcD, ApcF, or ApcE, emitting at 680 nm (APC_{680}). These terminal emitters function as spectral bridges between PB and photosystems. The third APC cylinder contains only $\alpha\beta$APC trimers emitting at 660 nm. All of these pigment−proteins (phycobiliproteins) are bound together by several types of linker peptides.[22−26] PBs form a rather efficient antenna system, funneling more than 90% of the captured energy via APC_{680} to the lower energy Chls within PSI and PSII, where the photochemical reactions are performed.[22,23,27,28] A schematic overview of the PB organization is given in Figure 1 together with a global description of previously resolved excitation energy transfer times in *Synechocystis*.[13,26,29,30]

It is already known that qE_{cya} does not occur in the outer rods that contain the C-PC pigments thanks to various mutant studies.[8,13,15,18] This has just been confirmed by in vitro reconstitution experiments showing that OCP^r can bind to PB containing only the core, thereby completely quenching its fluorescence. In contrast, OCP^r is unable to quench the fluorescence of PB containing only PC rods.[11] Therefore, the quenched species should be either an APC_{660} or an APC_{680} pigment in the APC core.[18,20] It is one of the goals of the present study to find out where exactly in the PB qE_{cya} takes place. The differences in the fluorescence maxima of the various pigments should facilitate the analysis of the ultrafast fluorescence data sets and enable the identification of the quenching site.

qE_{cya} is accompanied by a spectral and conformational change of the carotenoid hECN bound to OCP but it is unknown what the molecular quenching mechanism is. By comparing the spectrally resolved picosecond fluorescence kinetics in the presence and absence of qE_{cya}, we intend to determine the rate of quenching which should then hopefully shed light on the underlying physical mechanism, which is also still unknown.

We have performed picosecond fluorescence measurements on *Synechocystis* WT cells and cells of the OverOCP and ΔOCP mutants in (a) the unquenched state, (b) the quenched state, and (c) the state after recovering from quenching. A compartmental model was constructed to describe excitation-energy transfer and trapping in *Synechocystis* using target analysis. From the target analysis, it was concluded where qE_{cya} takes place and what the (molecular) rate of quenching is. This also allowed us to draw conclusions about the mechanism of quenching and to calculate which percentage of the PB excitations reach PSI and PSII in the presence of qE_{cya}.

MATERIALS AND METHODS

Strains and Growth Conditions. The construction of the mutants without OCP protein (ΔOCP) and with overexpressed OCP protein (OverOCP) was described before (for details see refs 9, 10).

WT and mutant cells were grown photoautotrophically in a modified BG11 medium[31] containing also 10 mM $NaHCO_3$ and twice the concentration of sodium nitrate. Cells were shaken in a rotary shaker (45 rpm) at 30 °C and illuminated by white lamps at 40 $\mu mol \cdot m^{-2} \cdot s^{-1}$. Mutants were grown in the presence of antibiotics (spectinomycin 25 $\mu g \cdot mL^{-1}$, streptomycin 10 $\mu g \cdot mL^{-1}$). All cells were grown in 250-mL flasks with a growing volume of 60 mL, and maintained in the logarithmic growth phase with optical densities at 800 nm (OD_{800}) between 0.6 and 0.8 (scattering) by refreshing the medium every 2 to 3 days.

To improve the signal-to-noise ratio of the time-resolved fluorescence measurements, cell suspensions were concentrated 3−5 times. The final suspensions were dark-adapted for 5 min before performing the fluorescence measurements.

Fluorescence Measurements. *1. Steady-State Fluorescence.* Steady-state fluorescence spectra were recorded with a Jobin Yvon Fluorolog FL3−22 spectrofluorimeter and corrected for wavelength-dependent sensitivity of the detection and fluctuations in lamp output. The excitation wavelength was 590 nm; a bandwidth of 5 nm was used for excitation and emission. Fluorescence emission spectra were recorded using a step size of 0.5 nm. Cell suspensions were diluted to a final Chl concentration of 1.0 $\mu g \cdot mL^{-1}$ and measured in a cuvette with a

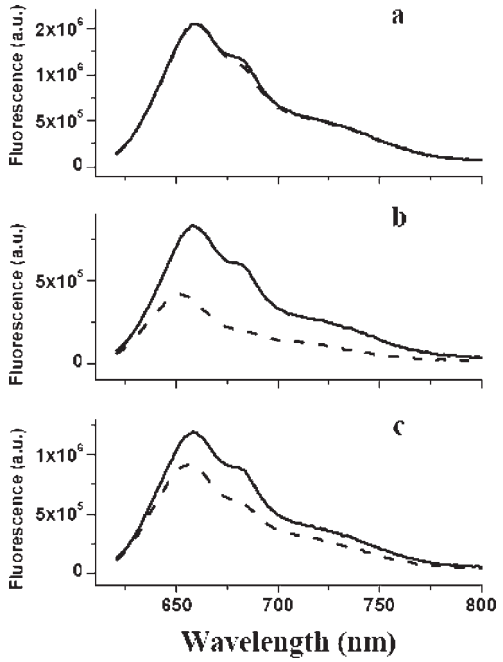

Figure 2. Room-temperature fluorescence spectra upon 590 nm excitation of cells (1 μg Chl/mL) before (solid lines) and after (dashed lines) blue-green light illumination (220 $\mu E \cdot m^{-2} \cdot s^{-1}$), (a) ΔOCP, (b) OverOCP, (c) WT.

3-mm light path to avoid significant self-absorption. Cells were quenched by illuminating with 500 nm light at ~220 $\mu E \cdot m^{-2} \cdot s^{-1}$ for 10 min at 20 °C and emission spectra were recorded immediately after quenching.

2. Time-Resolved Fluorescence. Time-resolved fluorescence spectra were recorded with a subpicosecond streak-camera system combined with a grating (50 grooves/mm, blaze wavelength 600 nm) with the central wavelength set at 700 nm, having a spectral width of 260 nm (for details see ref 32). Excitation light was vertically polarized, the spot size diameter was typically ~100 μm, and the laser repetition rate was 250 kHz. The detector polarizer was set at magic angle orientation. Great care was taken to minimize the path length (typical ~100 μm) to allow measurements on high-concentration samples (OD_{680} > 3) without significant self-absorption. Two excitation wavelengths were used: 590 and 400 nm. To avoid photodamage and to induce qE_{cya} in the entire cuvette (see below), the sample was stirred with a magnetic stirring bar (rate ~10 Hz) and the laser power at 590 nm was adjusted to 15 ± 3 μW. At 400 nm, the power was adjusted to ~30 ± 3 μW. Images of 800 ps and 2 ns time windows were obtained for each sample and corrected for background and photocathode shading, and then sliced up into traces of 4 nm width.

For both excitation wavelengths, the instrument response function (IRF) was described with a double Gaussian, consisting of a Gaussian of ~9 ps fwhm (90% of IRF area) on top of a Gaussian of 100 ps fwhm (10% of IRF area).

For measuring time-resolved fluorescence of cells during quenching, an actinic white light source was used in combination with a 500 nm broad band filter (K50) giving an intensity of ~350 $\mu E \cdot m^{-2} \cdot s^{-1}$. The volume used for fluorescence excitation/detection was spatially well separated from the actinic light beam (a cylinder of ~5 mm diameter × 1 cm length); the entire volume of the sample was 4 mL. One measurement was performed as follows: First, after 5 min of dark adaptation of the cells, fluorescence streak images were recorded for unquenched cells. Then, cells were quenched by actinic illumination at 20 °C for 1 h (to obtain the maximal quenching possible at the light intensity used) while stirring; during subsequent measurements on quenched cells, the actinic illumination was kept on to maintain the quenched state. Finally, streak images were recorded after allowing the cells to fully recover from qE_{cya} for 1 h in the dark. At 20 °C, fluorescence recovery is slower than at 32 °C, and for the overOCP strain, it can take almost 1 h. ΔOCP, being the perfect control sample because it does not show qE_{cya}, was measured in exactly the same way as WT and Over OCP cells. A high signal-to-noise ratio was achieved by averaging 100 single images, each obtained after analog integration of 10 exposures of 1.112 s. Measurements were performed at room temperature (about 20 °C) and lasted 3 h for each sample.

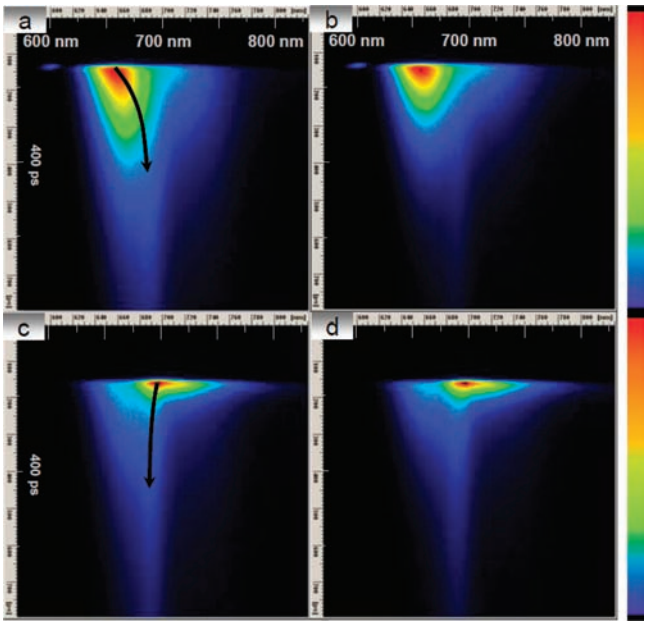

Figure 3. Streak-camera images of unquenched (a and c) and quenched (b and d) OverOCP cells. These images represent the fluorescence intensity (using a linear color gradient) as a function of time (vertical axis) and wavelength (horizontal axis); every vertical line represents a time trace of fluorescence at the corresponding wavelength, while every horizontal line reflects a fluorescence emission spectrum after a certain delay time. In panels a and b, C-Phycocyanin was selectively excited at 590 nm, and in panels c and d, Chls were selectively excited at 400 nm; all time-resolved fluorescence measurements represented in this work were repeated at least three times with cells grown on different days.

3. Data Analysis. Data obtained with the streak-camera setup were first globally analyzed with the R package TIMP (for details see refs 33, 34). The methodology of global analysis is described in van Stokkum et al.:[35] with global analysis, the data were fitted as a sum of exponential decays convolved with an IRF and the amplitudes of each decay component as a function of wavelength are called decay-associated spectra (DAS). Subsequently, 'target analysis' was performed as described in the Supporting Information.

RESULTS

1. Steady-State Fluorescence. Steady-state fluorescence spectra of unquenched cells of WT, OverOCP, and ΔOCP were recorded upon 590 nm excitation (Figure 2). The spectra are very similar for all unquenched cells, showing two main peaks at 660 and 680 nm. The 660 nm maximum originates from APC_{660} and the one at 680 nm from APC_{680} and/or Chl. Figure 2 also shows the spectra after 10 min of illumination with 220 $\mu E \cdot m^{-2} \cdot s^{-1}$ blue-green light. For WT cells, this causes ~20%

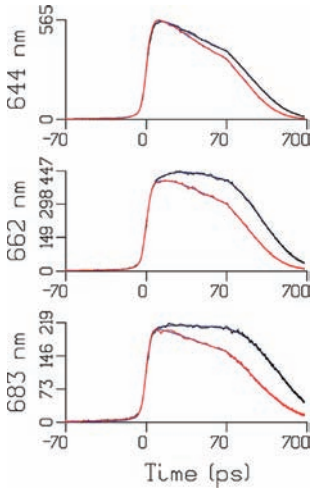

Figure 4. Emission traces at 644, 662, and 683 nm of unquenched (black) and quenched (red) OverOCP upon 590 nm excitation. Note that the time axis is linear until 70 ps, and logarithmic thereafter. Blue lines indicate the global analysis fit with five lifetimes.

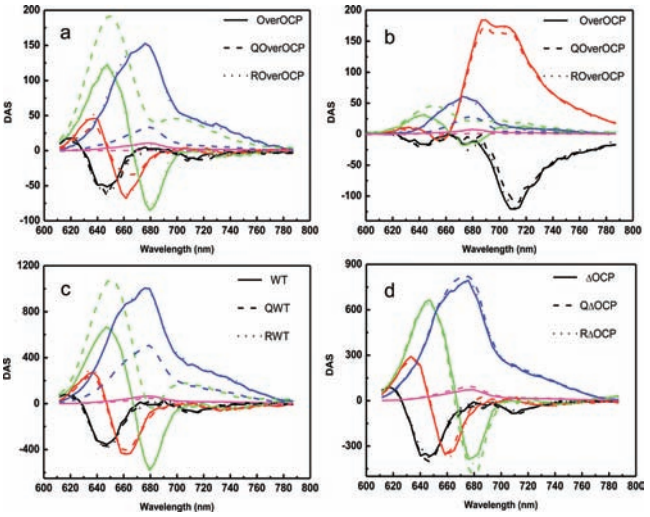

Figure 5. DAS of intact cells of OverOCP (a and b), WT (c), and ΔOCP (d), after 590 nm (a,c,d) or 400 nm excitation (b). Spectra correspond to 'unquenched' (solid), 'quenched' (dashed), labeled with Q or 'recovered' cells (dotted), labeled with R.

fluorescence quenching, while for OverOCP, more than 50% quenching occurs. As expected, no quenching is observed for ΔOCP cells.

2. Time-Resolved Fluorescence. To determine the quenching kinetics, time-resolved fluorescence of mutant and WT cells was measured with a picosecond streak-camera system. The cells were studied in three different states: before illumination (unquenched), after illumination with strong quenching-inducing light (quenched) (illumination is continued during the measurement), and 1 h after switching off the quenching light (recovered). Either 590 nm laser pulses were used, exciting mainly C-PC (Figure 3a,b), or 400 nm pulses, exciting mainly Chls in PSI and PSII (Figure 3c,d). Figure 3a shows that the spectrum is shifting to longer wavelengths in time (red-shifting) after 590 nm excitation, which is due to downhill excitation energy transfer (EET). In contrast, Figure 3c shows that after 400 nm excitation the spectrum is slightly blue-shifting (indicated by the black arrow). The blue-shift is due to the fact that long-wavelength PSI fluorescence is shorter-lived than PSII fluorescence that contributes more at shorter wavelengths. A comparison of panels a and b in Figure 3 clearly shows that the fluorescence of unquenched OverOCP (Figure 3a) is longer-lived than that of quenched OverOCP (Figure 3b). The WT cells also show faster decay of the excited state after induction of qE_{cya}, albeit less pronounced. The quenching appears to be completely reversible, meaning that the fluorescence streak images of cells that are recovered from qE_{cya} are virtually identical to the ones before qE_{cya}. As expected, no significant changes are observed for the ΔOCP cells. Upon 400 nm excitation, the effects of qE_{cya} are far less noticeable for all cell types and only a minor decrease in intensity can be observed on the short-wavelength side for WT and OverOCP cells, where PBs dominate the fluorescence.

3. Modeling Results. To get quantitative information from these images, both global analysis and target analysis were performed. Global analysis provides a minimal mathematical description of the data revealing the wavelength dependence of EET and excitation trapping. On the basis of this kinetic information, combined with a priori knowledge of the photosynthetic system, target analysis was used to construct a specific compartmental model with corresponding rate constants to obtain a realistic description of the system. By exploring the model that fits best to the data, kinetic constants for the various processes (energy transfer, trapping and quenching) could be determined.

Table 1. Lifetimes of DAS[a]

Lifetimes (ps)	λex	tau 1	tau 2	tau 3	tau 4	tau 5
OverOCP/ROverOCP	590 nm	8	36	128	204	>500 ps
QOverOCP	590 nm	8	26	105	301	>500 ps
OverOCP/ROverOCP	400 nm	6	22	134	232	>500 ps
QOverOCP	400 nm	6	23	120	367	>500 ps
WT/RWT	590 nm	9	39	122	195	>500 ps
QWT	590 nm	8	36	116	239	>500 ps
ΔOCP/QΔOCP/RΔOCP	590 nm	8	38	121	205	>500 ps

[a] Lifetimes estimated from global analysis of the fluorescence data obtained for the various cells in different states. The colors of the lifetimes correspond to the colors of the DAS in Figure 5. And the samples were named the same as in Figure 5.

3.1. Global Analysis. ***3.1.1. OverOCP.*** Typical unquenched (black) and quenched (red) traces for excitation at 590 nm are depicted in Figure 4 and quenching appears to be particularly well visible at 662 and 683 nm.

Global analysis of 50 emission traces of OverOCP cells reproducibly required five lifetimes. The results are shown in Figure 5a and corresponding lifetimes are given in Table 1. Induction of qE_{cya} by strong blue-green light leads to marked changes of several DAS. After switching off the blue-green light, quenching effects disappeared completely in approximately 1 h at 20 °C, demonstrating the reversibility of qE_{cya}. After cells had "recovered" from qE_{cya}, the DAS were identical to those before qE_{cya}.

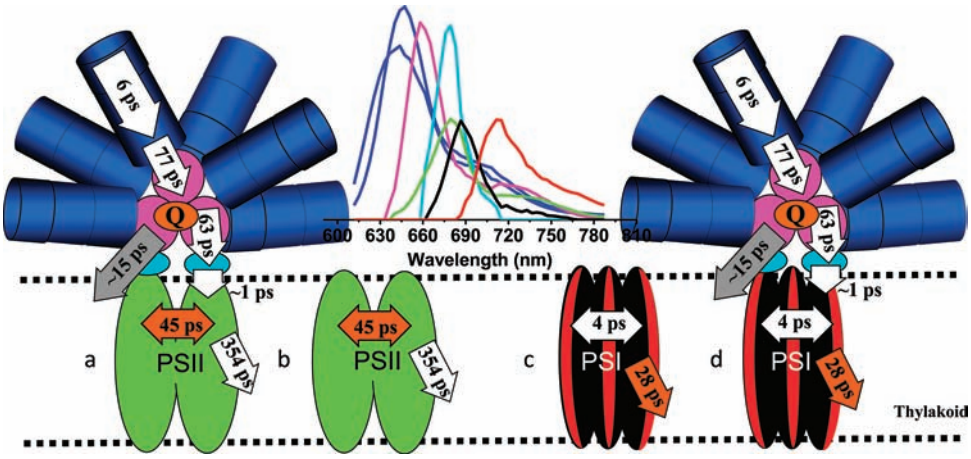

Figure 6. Schematic model showing the downhill energy transfer and trapping processes in *Synechocystis* with characteristic transfer times (a transfer time is defined as 1/transfer rate). SAS (fitting results) are shown in colors that refer to the protein complexes holding the corresponding pigments. Inverse rates of uphill energy transfer are omitted for clarity but can be found in the Supporting Information (Figure SI.2).

The black DAS in Figure 5 reflect excitation equilibration (predominantly downhill EET) in C-PC with a time constant of 8 ps, displaying a positive/negative signature, characteristic for energy transfer. The acceptor states have a higher dipolar strength than the donor states (see, e.g., ref 36) leading to a predominantly negative DAS. These DAS and their corresponding lifetimes remain unaltered upon qE_{cya} induction, showing that the corresponding transfer process is not influenced by quenching.

The red DAS with ~30 ps lifetime to a large extent reflect downhill EET from C-PC to APC_{660}. They are only slightly influenced by quenching because the changes in lifetime and DAS are rather small, especially when compared to the changes observed for the slower components.

The green DAS for unquenched and recovered cells with a lifetime of 130 ps reflect to a large extent EET from APC_{660} to APC_{680} + Chls. Like the ~30 ps component, they have the characteristic conservative shape with positive amplitude at short wavelengths and negative amplitude at longer wavelengths, meaning that excited-state population disappears from pigments fluorescing somewhat above 650 nm to pigments with a fluorescence maximum somewhat below 680 nm. This component is strongly influenced by the quenching; the lifetime decreases and the shape changes drastically. It loses its characteristic conservative transfer character, indicating that excitations on APC_{660} are quenched, and this leads to a shortening of the APC_{660} excited-state lifetime and a decrease in energy transfer. From these DAS it is not directly clear which percentage of the APC pigments is quenched and what the quenching rate is. These issues will be addressed below using the target analysis approach.

The dark blue DAS with 200−300 ps lifetime reflect excitation trapping by the RCs (charge separation). The DAS represents an equilibrated excitation distribution over C-PC, APC_{660}, APC_{680}, and Chls. Upon induction of qE_{cya}, the intensity of this component decreases drastically, due to the fact that many excitations are already quenched on APC_{660} before they can reach APC_{680} and Chls.

The cyan DAS with lifetimes above 500 ps have very small amplitudes. The lifetime is not well determined using the 800 ps time window; it can be varied from 600 ps to a few nanoseconds in the fit without influencing shape and position of the DAS. In data sets obtained with a 2 ns time window, the corresponding lifetime was determined to be ~700 ps. These DAS probably reflect competition between secondary charge separation and charge recombination (see, e.g., ref 37), which explains why its amplitude decreases upon quenching.

Global analysis of the results that are obtained upon 400 nm excitation leads to the DAS that are shown in Figure 5b. Using 400 nm pulses, excitations are mainly created in PSI and PSII and only 10% is created in PB,[30] leading to the fluorescence on the short-wavelength side of the image. The latter excitations give rise to the same DAS and quenching kinetics as the excitations created by 590 nm laser pulses (see Figure 5b). The dominating component of 22 ps (red DAS in Figure 5b) represents emission from Chls in PSI,[30,38,39] which appears to be hardly quenched.

3.1.2. WT and ΔOCP. The DAS that are obtained for unquenched WT and ΔOCP cells (see Figure 5, panels c and d, respectively) are virtually identical to those obtained for unquenched OverOCP cells. This shows that the organization of the photosynthetic system is identical in all cases, but also it testifies to the high reproducibility of both measurement and analysis. The fluorescence kinetics of ΔOCP cells are hardly affected by illumination with strong blue-green light, but for WT cells, similar changes are induced as for OverOCP cells, although the effects of qE_{cya} are less pronounced. EET within the C-PC rods and from C-PC to APC are nearly unaffected in WT cells since the 2 DAS with the shortest lifetimes remain nearly the same. The third DAS, which is conservative in the absence of quenching, becomes strongly nonconservative, again reflecting quenching of APC_{660}. However, the strong dip around 680 nm indicates that still a substantial amount of EET toward APC_{680} and Chls takes place, also explaining why the fourth and fifth DAS decrease less in intensity for WT than for OverOCP. It is not immediately clear whether a larger fraction of PB remains unquenched as compared to OverOCP or whether the quenching rate is smaller. This issue will be addressed below.

In summary, global analysis of the presented time-resolved fluorescence data indicates that APC_{660} is quenched directly in vivo. However, it is not clear which fraction of the PB is quenched and what the rate of quenching is. To resolve these issues, target analysis was performed.

3.2. Target Analysis. It is known that PBs can transfer energy to both PSI and PSII.[27,28] Thus, a good model requires the presence

of PB coupled to PSII (PB−PSII) and to PSI (PB−PSI). To obtain acceptable fitting results, it was discovered that the amount of excitations being transferred from PB to PSII and PSI had to be rather similar (for more details see Supporting Information). PB was allowed to be quenched or unquenched and the fraction of quenched PB was included as a free fitting parameter. Quenched PB−PSII and PB−PSI are shown in Figure 6, whereas the unquenched versions are omitted from the figure for clarity. It has been reported that also uncoupled PB should be present,[29] but since the corresponding lifetime of 1.2−1.5 ns was not observed in our study, their amount was considered to be insignificant.

A correct description of the 400 nm data requires the presence of two additional pigment−protein structures: PSII and PSI without any coupled PBs (schematic structures of PSII and PSI are also included in Figure 6). Details about the fitting and input parameters are shown in the Supporting Information (Figure SI.2 and Table SI.1). The SAS resulting from the analysis are assigned based on the positions of their maxima: the two blue SAS correspond to short- and long wavelength forms of C-PC (here named PC-S and PC-L, respectively); the magenta SAS with maximum around 660 nm corresponds to APC_{660}; the cyan SAS and the green SAS with maximum around 680 nm correspond to APC_{680} and Chls in PSII, respectively. The black and red SAS originate from bulk Chls (688 nm) and red Chls (712 nm) in PSI, respectively, which is in perfect agreement with previous reports on isolated PSI.[38,40] As pointed out in the Supporting Information, also energy transfer rates are in agreement with reports on PSI, PSII, and PBs and subcomplexes thereof and the same is true for the fluorescence spectra (SAS) of the various pigments.

To determine in which of the different pigment pools the blue-green light-induced quenching takes place, one additional decay rate constant k_Q (reflecting the quenching) was added in turn to the various compartments and the data for the quenched cells was fitted keeping all other rate constants the same as for the unquenched cells. The results were unequivocal: only quenching of the APC_{660} compartment leads to a satisfactory fit of the data and the corresponding quenching rate is $66 \pm 15\ ns^{-1}$ for OverOCP. Putting the quencher in another compartment resulted in fits of lesser quality or led to unrealistic SAS. Another important finding was that not all PBs are quenched. For OverOCP, the percentage of quenched PBs was found to be ∼72%.

With the same model, the data on WT cells could be fitted equally well, the main difference being that only ∼29% of all PBs appeared to be quenched whereas the quenching rate was $54\ ns^{-1}$ rather similar to that of OverOCP. This explains why, in steady-state spectra, the quenching ratio in WT cells is only about one-third of that in OverOCP cells.

For the ΔOCP mutant, the same target model was successfully applied (results not shown) for all three measuring states (before, during, and after applying high intensity blue-green light) and the results are similar to those for unquenched WT and OverOCP cells.

DISCUSSION

1. The Location, Rate, and Efficiency of qE_{cya}. It was demonstrated before with steady-state fluorescence measurements on various *Synechocystis* mutants and in vitro reconstitution experiments that quenching takes place in the APC core of the PB[9,11,13,15] and our current data confirm this. However, due to fast EET from APC_{660} to APC_{680}/Chls it could not be determined before whether APC_{660} or APC_{680}[20] was quenched and also the quenching rate remained unknown. It is now revealed that quenching takes place at the level of APC_{660} and not APC_{680}. The rate of quenching of the APC_{660} pool turns out to be $66 \pm 15\ ns^{-1}$ (which is equivalent to $(16 \pm 4\ ps)^{-1}$). This is extremely fast and leads to efficient quenching. From the parameters obtained with the target analysis, it can be concluded that in the presence of qE_{cya}, 80% of the excitations that are harvested by a quenched PB are dissipated as heat before reaching PSII and PSI (see Supporting Information). Our results indicate that both PSI and PSII are protected. However, not all PBs are in the quenched state. The number of quenched PBs depends on the ratio OCP^r to PB[11]. In WT cells, there is only 1 OCP per 2−3 PB. Moreover, not all OCP is expected to be in the OCP^r state in the used light conditions, although the exact amount of activated OCP is unknown. Indeed, we found that only 29% of the PBs were quenched for WT cells. For OverOCP cells, the concentration of OCP is about 7- to 8-fold higher than in WT, meaning more than 2−3 OCP per PB[21]. Consistently, the number of quenched PBs is substantially higher, namely, 72%.

2. The Mechanism of qE_{cya} at the Molecular Level. Our present study has disclosed that one of the APC_{660} pigments is directly quenched (from now on we call this quenched pigment APC^Q_{660}). The overall quenching rate of the APC_{660} pool appears to be $66 \pm 15\ ns^{-1}$ or $(16 \pm 4\ ps)^{-1}$. Since there are approximately 66 APC_{660} pigments present in one PB core, the molecular quenching rate of APC^Q_{660} is at most $(0.24 \pm 0.06\ ps)^{-1}$, corresponding to 16/66 ps in case EET within the APC660 pool is infinitely fast. In the case of infinitely fast EET, the probability that the excitation is on the quenched pigment is 1/66 which slows down the molecular quenching rate by a factor of 66. Slower EET requires an even faster quenching rate (see, e.g., ref 37).

It has been hypothesized that the C-terminal OCP domain, by interacting with the center of an APC trimer, may bring the carotenoid into proximity of the APC chromophores, whereas light-induced carotenoid changes could then regulate the interaction between the carotenoid and the APC chromophores (either α84 or β84).[10] Support for this hypothesis comes from the fact that the C-terminal domain of OCP is structurally similar to the 7.8 kDa core linker protein that is bound within the central aperture of the APC trimer and directly interacts with the β84 chromophores of two APC subunits. The present findings indeed confirm the direct quenching of one of the APC chromophores and the ultrafast quenching rate suggests extremely strong coupling between one of the APC chromophores and the OCP carotenoid hECN.

One could envision several carotenoid-induced quenching mechanisms occurring based on the analogy of chlorophyll quenching by carotenoids: (1) excitonic coupling[41−43] between APC^Q_{660} and hECN, (2) EET from APC^Q_{660} to the S_1 state of hECN,[44,45] (3) electron transfer from hECN to APC^Q_{660}.[46] The same three mechanisms were also recently identified for tetrapyrrole singlet excited state quenching by carotenoids in artificial systems.[47]

The fact that the quenching rate is faster than $(1\ ps)^{-1}$ rules out the first mechanism because the excited-state decay rate would be a weighted average of the excited-state decay rate of APC_{660} and of hECN in the absence of interaction.[43] Because the excited-state lifetime of hECN is above 1 ps and that of APC_{660} even above 1 ns, it is impossible to obtain an average lifetime which is 0.24 ps or even shorter.

It is more difficult to estimate whether EET from APC^{Q}_{660} to the S_1 state of hECN might happen with a rate of $(0.24 \pm 0.06\ ps)^{-1}$. Up to now, rates of EET from the lowest excited state of (B)Chls/bilins to the carotenoid S_1 state have not been measured for pigment−protein complexes. However, various studies have reported rates for EET from the carotenoid S_1 state to the lowest Q_y states of (bacterio)chlorophylls. Both types of rates are expected to be similar because the electronic coupling mechanism is the same, while mainly the relative ordering of the energy levels of both molecules differs in both cases. Carotenoid-to-BChl *a* energy transfer times involving the S_1 state were reported to be of the order of several picoseconds for light-harvesting complexes from purple bacteria.[48−52] This is an order of magnitude slower than the obtained quenching rate in the present study. A larger spread in transfer times was reported for Chl *a* containing light-harvesting complexes LHCII and CP29.[53−56] Whereas Croce et al. hardly observed any transfer from the S_1 state in LHCII from plants,[53] a time constant of ∼1 ps was reported by Gradinaru et al.,[54] whereas Walla et al. found several transfer times, ranging from ∼200 fs to over 7 ps.[55] For CP29, Croce et al. reported different transfer times for the different carotenoids in CP29,[56] the fastest being 700 fs, whereas Gradinaru et al. found a time of around 1 ps.[54]

It is important to note that a transient absorption study was performed on a model system made up of a zinc phtalocyanine (*Pc*) molecule (similar to Chl) covalently linked to carotenoids with 9, 10, or 11 conjugated carbon−carbon double bonds.[57] By increasing the number of double bonds, the S_1 energy level becomes lower than the lowest excited singlet energy level of the *Pc* molecule. EET could be observed from *Pc* to the Car in the case of 10 and 11 conjugated double bonds and the transfer rates varied from $(56\ ps)^{-1}$ to $(17\ ps)^{-1}$, depending on solvent polarity and conjugation length, that is, far slower than the observed quenching rate in the present study. We conclude that most of the experimentally obtained transfer rates are slower or even far slower than the lower limit for the quenching rate of $(0.24 \pm 0.06\ ps)^{-1}$ but we cannot entirely exclude that EET from APC^{Q}_{660} to the S_1 state of hECN might be responsible for qE_{cya}.

Finally, it has been reported that in plants nonphotochemical quenching can occur via charge transfer within a closely coupled excited pair of a Chl *a* molecule and a zeaxanthin carotenoid molecule with a time constant between 0.1 and 1.0 ps, leading to fluorescence quenching of Chl.[46,58] The rate of $(\sim 0.24 \pm 0.06\ ps)^{-1}$ for APC quenching in cyanobacteria falls nicely within this interval. Therefore, based on the available data, it appears most likely that charge transfer from the red form of hECN in OCP to APC^{Q}_{660} in the PB core is responsible for the blue-green light-induced nonphotochemical quenching in cyanobacteria.

■ ASSOCIATED CONTENT

Supporting Information. Scheme of the model, inputs and fitting parameters of target analysis and fitting quality. This material is available free of charge via the Internet at http://pubs.acs.org.

■ AUTHOR INFORMATION

Corresponding Author
Herbert.vanAmerongen@wur.nl

■ ACKNOWLEDGMENT

We thank Dr. S. Laptenok (Ecole Polytechnique, 91128 Palaiseau, France) and J. Snellenburg (VU Amsterdam University) for help with the use of the TIMP package, C. Wolfs (Wageningen UR) for help in growing the cells and Arie van Hoek (Wageningen UR) for technical support. This work was supported by a fellowship to L.T. from the Graduate School Experimental Plant Sciences (EPS), Wageningen, The Netherlands, by the Dutch Ministry of ELI through the BioSolar Cells Project and by the European community via the HARVEST project.

■ REFERENCES

(1) Aro, E.-M.; Virgin, I.; Andersson, B. *Biochim. Biophys. Acta, Bioenerg.* **1993**, *1143*, 113–134.
(2) Tyystjarvi, E. *Coord. Chem. Rev.* **2008**, *252*, 361–376.
(3) Vass, I. *Physiol. Plant.* **2011**, *142*, 6–16.
(4) Horton, P.; Ruban, A. V.; Walters, R. G. *Annu. Rev. Plant Phys.* **1996**, *47*, 655–684.
(5) Niyogi, K. K. *Annu. Rev. Plant Phys.* **1999**, *50*, 333–359.
(6) Kirilovsky, D. *Photosynth. Res.* **2007**, *93*, 7–16.
(7) El Bissati, K.; Delphin, E.; Murata, N.; Etienne, A. L.; Kirilovsky, D. *Biochim. Biophys. Acta, Bioenerg.* **2000**, *1457*, 229–242.
(8) Rakhimberdieva, M. G.; Stadnichuk, I. N.; Elanskaya, T. V.; Karapetyan, N. V. *FEBS Lett.* **2004**, *574*, 85–88.
(9) Wilson, A.; Ajlani, G.; Verbavatz, J. M.; Vass, I.; Kerfeld, C. A.; Kirilovsky, D. *Plant Cell* **2006**, *18*, 992–1007.
(10) Wilson, A.; Punginelli, C.; Gall, A.; Bonetti, C.; Alexandre, M.; Routaboul, J. M.; Kerfeld, C. A.; van Grondelle, R.; Robert, B.; Kennis, J. T. M.; Kirilovsky, D. *Proc. Natl. Acad. Sci. U.S.A.* **2008**, *105*, 12075–12080.
(11) Gwizdala, M.; Wilson, A.; Kirilovsky, D. *Plant Cell* **2011**, *23*, 2631–2643.
(12) Boulay, C.; Wilson, A.; D'Haene, S.; Kirilovsky, D. *Proc. Natl. Acad. Sci. U.S.A.* **2010**, *107*, 11620–11625.
(13) Scott, M.; McCollum, C.; Vasil'ev, S.; Crozier, C.; Espie, G. S.; Krol, M.; Huner, N. P. A.; Bruce, D. *Biochemistry* **2006**, *45*, 8952–8958.
(14) Rakhimberdieva, M. G.; Bolychevtseva, Y. V.; Elanskaya, I. V.; Karapetyan, N. V. *FEBS Lett.* **2007**, *581*, 2429–2433.
(15) Rakhimberdieva, M. G.; Vavilin, D. V.; Vermaas, W. F. J.; Elanskaya, I. V.; Karapetyan, N. V. *Biochim. Biophys. Acta, Bioenerg.* **2007**, *1767*, 757–765.
(16) Wilson, A.; Boulay, C.; Wilde, A.; Kerfeld, C. A.; Kirilovsky, D. *Plant Cell* **2007**, *19*, 656–672.
(17) Boulay, C.; Abasova, L.; Six, C.; Vass, I.; Kirilovsky, D. *Biochim. Biophys. Acta, Bioenerg.* **2008**, *1777*, 1344–1354.
(18) Rakhimberdieva, M. G.; Elanskaya, I. V.; Vermaas, W. F. J.; Karapetyan, N. V. *Biochim. Biophys. Acta, Bioenerg.* **2010**, *1797*, 241–249.
(19) Wilson, A.; Kinney, J. N.; Zwart, P. H.; Punginelli, C.; D'Haene, S.; Perreau, F.; Klein, M. G.; Kirilovsky, D.; Kerfeld, C. A. *J. Biol. Chem.* **2010**, *285*, 18364–18375.
(20) Rakhimberdieva, M. G.; Kuzminov, F. I.; Elanskaya, I. V.; Karapetyan, N. V. *FEBS Lett.* **2011**, *585*, 585–589.
(21) Kirilovsky, D.; Kerfeld, C. A. *Biochim. Biophys. Acta* **2011**, DOI:10.1016/j.bbabio.2011.04.013.
(22) Glazer, A. N. *Biochim. Biophys. Acta* **1984**, *768*, 29–51.
(23) Grossman, A. R.; Schaefer, M. R.; Chiang, G. G.; Collier, J. L. *Microbiol. Rev.* **1993**, *57*, 725–749.
(24) MacColl, R. *J. Struct. Biol.* **1998**, *124*, 311–334.
(25) Adir, N. *Photosynth. Res.* **2005**, *85*, 15–32.
(26) Arteni, A. A.; Ajlani, G.; Boekema, E. J. *Biochim. Biophys. Acta, Bioenerg.* **2009**, *1787*, 272–279.
(27) Ashby, M. K.; Mullineaux, C. W. *Photosynth. Res.* **1999**, *61*, 169–179.
(28) Dong, C.; Tang, A.; Zhao, J.; Mullineaux, C. W.; Shen, G.; Bryant, D. A. *Biochim. Biophys. Acta, Bioenerg.* **2009**, *1787*, 1122–1128.

(29) Bittersmann, E.; Vermaas, W. *Biochim. Biophys. Acta* **1991**, *1098*, 105–116.
(30) Krumova, S. B.; Laptenok, S. P.; Borst, J. W.; Ughy, B.; Gombos, Z.; Ajlani, G.; van Amerongen, H. *Biophys. J.* **2010**, *99*, 2006–2015.
(31) Rippka, R.; Deruelles, J.; Waterbury, J. B.; Herdman, M.; Stanier, R. Y. *J. Gen. Microbiol.* **1979**, *111*, 1–61.
(32) Stokkum, I. H. M.; Oort, B.; Mourik, F.; Gobets, B.; Amerongen, H. In *Biophysical Techniques in Photosynthesis*; Aartsma, T. J., Matysik, J., Eds.; Springer: Netherlands: 2008; Vol. 26, pp 223−240.
(33) Laptenok, S. P.; Borst, J. W.; Mullen, K. M.; van Stokkum, I. H. M.; Visser, A. J. W. G.; van Amerongen, H. *Phys. Chem. Chem. Phys.* **2010**, *12*, 7593–7602.
(34) Mullen, K. M.; van Stokkum, I. H. M. *J. Stat. Software* **2007**, *18*, 1–46.
(35) van Stokkum, I. H. M.; Larsen, D. S.; van Grondelle, R. *Biochim. Biophys. Acta, Bioenerg.* **2004**, *1657*, 82–104.
(36) van Amerongen, H..; Valkunas, L.; van Grondelle, R. *Photosynthetic Excitons*; World Scientific Publishing Co.Pte.Ltd.: River Edge, NJ, 2000.
(37) Broess, K.; Trinkunas, G.; van Hoek, A.; Croce, R.; van Amerongen, H. *Biochim. Biophys. Acta, Bioenerg.* **2008**, *1777*, 404–409.
(38) Gobets, B.; van Grondelle, R. *Biochim. Biophys. Acta, Bioenerg.* **2001**, *1507*, 80–99.
(39) van Oort, B.; Amunts, A.; Borst, J. W.; van Hoek, A.; Nelson, N.; van Amerongen, H.; Croce, R. *Biophys. J.* **2008**, *95*, 5851–5861.
(40) Gobets, B.; van Stokkum, I. H. M.; van Mourik, F.; Dekker, J. P.; van Grondelle, R. *Biophys. J.* **2003**, *85*, 3883–3898.
(41) Lampoura, S. S.; Barzda, V.; Owen, G. M.; Hoff, A. J.; van Amerongen, H. *Biochemistry* **2002**, *41*, 9139–9144.
(42) Bode, S.; Quentmeier, C. C.; Liao, P. N.; Hafi, N.; Barros, T.; Wilk, L.; Bittner, F.; Walla, P. J. *Proc. Natl. Acad. Sci. U.S.A.* **2009**, *106*, 12311–12316.
(43) van Amerongen, H.; van Grondelle, R. *J. Phys. Chem. B* **2001**, *105*, 604–617.
(44) Ruban, A. V.; Berera, R.; Ilioaia, C.; van Stokkum, I. H. M.; Kennis, J. T. M.; Pascal, A. A.; van Amerongen, H.; Robert, B.; Horton, P.; van Grondelle, R. *Nature* **2007**, *450*, 575–U22.
(45) Young, A. J.; Phillip, D.; Ruban, A. V.; Horton, P.; Frank, H. A. *Pure Appl. Chem.* **1997**, *69*, 2125–2130.
(46) Holt, N. E.; Zigmantas, D.; Valkunas, L.; Li, X. P.; Niyogi, K. K.; Fleming, G. R. *Science* **2005**, *307*, 433–436.
(47) Kloz, M.; Pillai, S.; Kodis, G.; Gust, D.; Moore, T. A.; Moore, A. L.; van Grondelle, R.; Kennis, J. T. *J. Am. Chem. Soc.* **2011**, *133*, 7007–15.
(48) Walla, P. J.; Linden, P. A.; Hsu, C. P.; Scholes, G. D.; Fleming, G. R. *Proc. Natl. Acad. Sci. U.S.A.* **2000**, *97*, 10808–13.
(49) Zhang, J.-P.; Fujii, R.; Qian, P.; Inaba, T.; Mizoguchi, T.; Koyama, Y.; Onaka, K.; Watanabe, Y.; Nagae, H. *J. Phys. Chem. B* **2000**, *104*, 3683–3691.
(50) Polívka, T.; Pullerits, T.; Frank, H. A.; Cogdell, R. J.; Sundström, V. *J. Phys. Chem. B* **2004**, *108*, 15398–15407.
(51) Cong, H.; Niedzwiedzki, D. M.; Gibson, G. N.; LaFountain, A. M.; Kelsh, R. M.; Gardiner, A. T.; Cogdell, R. J.; Frank, H. A. *J. Phys. Chem. B* **2008**, *112*, 10689–703.
(52) Polivka, T.; Frank, H. A. *Acc. Chem. Res.* **2010**, *43*, 1125–1134.
(53) Croce, R.; Müller, M. G.; Bassi, R.; Holzwarth, A. R. *Biophys. J.* **2001**, *80*, 901–915.
(54) Gradinaru, C. C.; van Stokkum, I. H. M.; Pascal, A. A.; van Grondelle, R.; van Amerongen, H. *J. Phys. Chem. B* **2000**, *104*, 9330–9342.
(55) Walla, P. J.; Linden, P. A.; Ohta, K.; Fleming, G. R. *J. Phys. Chem. A* **2001**, *106*, 1909–1916.
(56) Croce, R.; Müller, M. G.; Caffarri, S.; Bassi, R.; Holzwarth, A. R. *Biophys. J.* **2003**, *84*, 2517–2532.
(57) Berera, R.; Herrero, C.; van Stokkum, I. H. M.; Vengris, M.; Kodis, G.; Palacios, R. E.; van Amerongen, H.; van Grondelle, R.; Gust, D.; Moore, T. A.; Moore, A. L.; Kennis, J. T. M. *Proc. Natl. Acad. Sci. U.S. A.* **2006**, *103*, 5343–5348.
(58) Ahn, T. K.; Avenson, T. J.; Ballottari, M.; Cheng, Y. C.; Niyogi, K. K.; Bassi, R.; Fleming, G. R. *Science* **2008**, *320*, 794–797.